Electronic Supplementary Material (ESI) for Journal of Materials Chemistry A.
This journal is © The Royal Society of Chemistry 2019

Hetero-Coupling Carbonate Hydroxide and Sulfide for Efficient and Robust Water Oxidation

Tang Tang,[ab] Wen-Jie Jiang,[a] Shuai Niu,[ab] Lu-Pan Yuan,[ab] Jin-Song Hu,[ab] and Li-Jun Wan*[ab]*

a. Beijing National Laboratory for Molecular Sciences (BNLMS), CAS Key Laboratory of Molecular Nanostructure and Nanotechnology, Institute of Chemistry, Chinese Academy of Sciences (CAS), Beijing 100190, China;

E-mail: hujs@iccas.ac.cn, wanlijun@iccas.ac.cn

b. University of Chinese Academy of Sciences, Beijing 100049, China.

This file includes Fig. S1-S16 and Table S1-S3

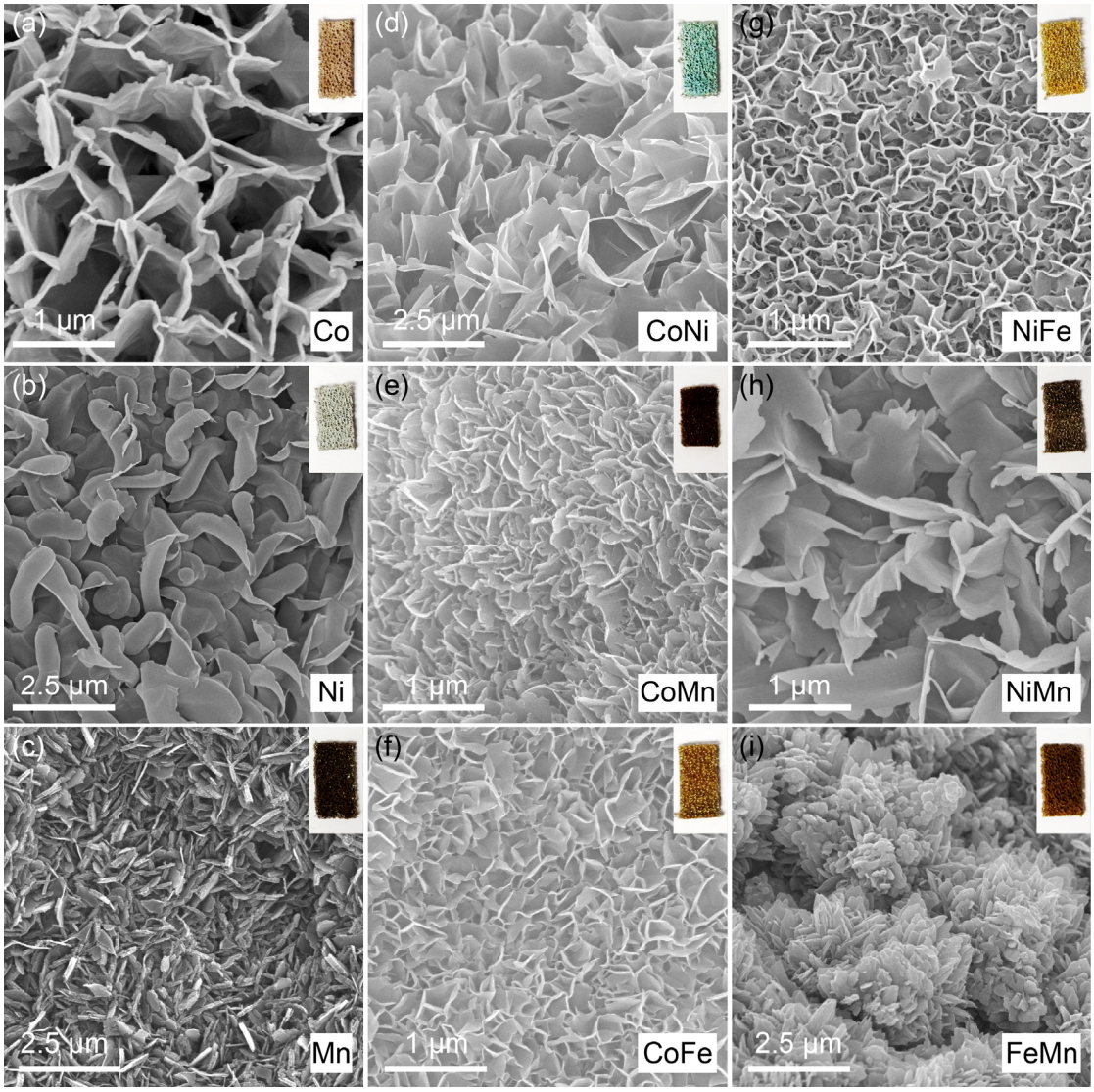

Fig. S1 SEM images of the various MCHs (insets: the corresponding digital photos): (a) Co, (b) Ni, (c) Mn, (d) CoNi, (e) CoMn, (f) CoFe, (g) NiFe, (h) NiMn, and (i) FeMn.

The structural flexibility and chemical versatility of MCH provide a promising possibility to alter their structure for enhanced electrocatalytic activities. To set out systematical investigation into the cooperative enhancement between different elements combination (Fe, Co, Ni, Mn) in the MCH structure for OER. A series of MCH arrays with mono- or bimetal compositions on the Ni foam are synthesized through a simple hydrothermal method and noted as MCH (where M represents the initial of metal name; Mn carbon hydroxide is noted as MnCH to distinguish from MCH). The absence of iron carbonate hydroxide is due to the fast hydrate of high concentration iron salt in alkalescent solution. The morphologies of all MCHs are revealed by scanning electron microscope (SEM). The corresponding digital photos (insets) in varied colours imply the successful construction of MCH. CCH with only Co source shows a honeycomb nanostructure (Fig. S1a). The nanosheet in NCH with only Ni source (Fig. S1b) shows an interlaced thin strip morphology. In contrast, MnCH exhibits a stacked morphology consisting of thick nanoplates (Fig. S1c), far different from CCH and NCH. Introducing second metal has an obvious influence on

the morphology of MCH. The honeycomb structure becomes flatter and larger after the introduction of Ni into CCH (Fig. S1d), integrating some features of NCH. This phenomenon is also observed in CMCH (Fig. S1e), which combines characteristics of both CCH and MnCH. The overall morphology is similar to MnCH but the nanosheets stay individually, resulting in a small but dense nanosheet array. Both CFCH (Fig. S1f) and NFCH (Fig. S1g) exhibit a porous structure consisting of small and interconnecting nanosheets. Introducing Mn into NCH only makes the nanosheets rougher (Fig. S1h). Distinctly, the introduction of Fe into MnCH changes the overall morphology (Fig. S1i), giving a flower-like structure consisting of thick interconnecting nanoplates for FMCH.

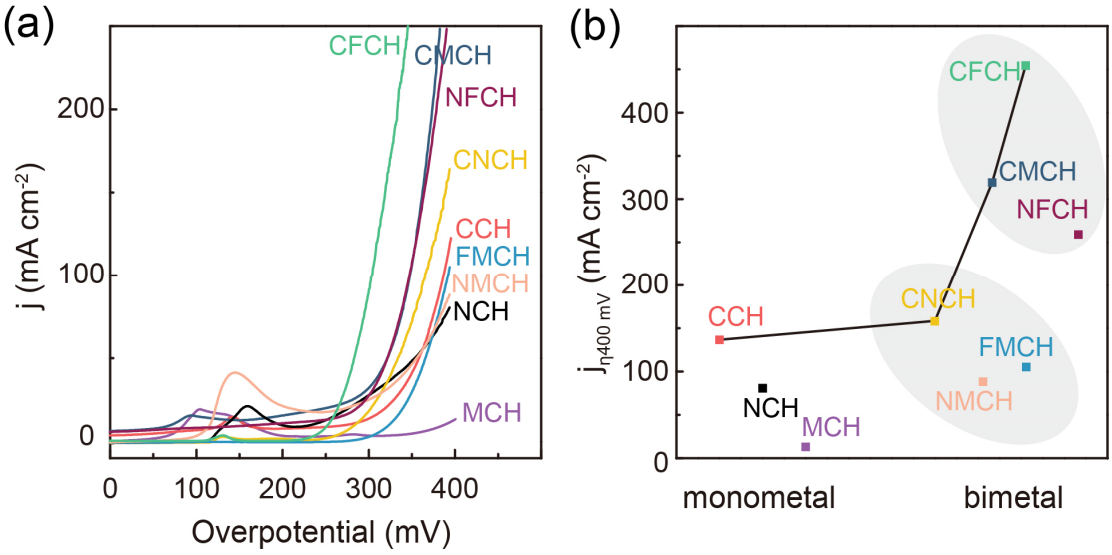

Fig. S2 (a) OER LSV curves of various MCHs. (b) Current density comparison of various MCHs under 400 mV overpotential.

OER activities of these MCHs are then investigated by polarization experiments with 90% iR-compensation (Fig. S2a). CCH shows the best performance among the three monometal MCHs. After introducing the second metal into the structure, the OER activities of three Co-based bimetal MCHs (CNCH, CMCH, and CFCH) are apparently increased as indicated by the appreciable negative-shift polarization curves. The current densities of these MCHs under an overpotential of 400 mV (η_{400}) are summarized as shown in Fig. S2b. It is clear that the bimetal Co-based MCHs show higher performance than original CCH. The combination of Co and Fe presents the best activity with low overpotentials of 252 and 304 mV at 10 and 100 mA cm^{-2}, respectively. The enhancement is also observed in bimetal Ni and Mn-based MCHs. These observations indicate efficient electronic engineering through cation regulation. The elemental combination in carbon hydroxides such as CoFe, CoMn, and NiFe generally enhances the performance for OER. This result may provide a guidance for the development of potential high performance OER electrocatalysts.

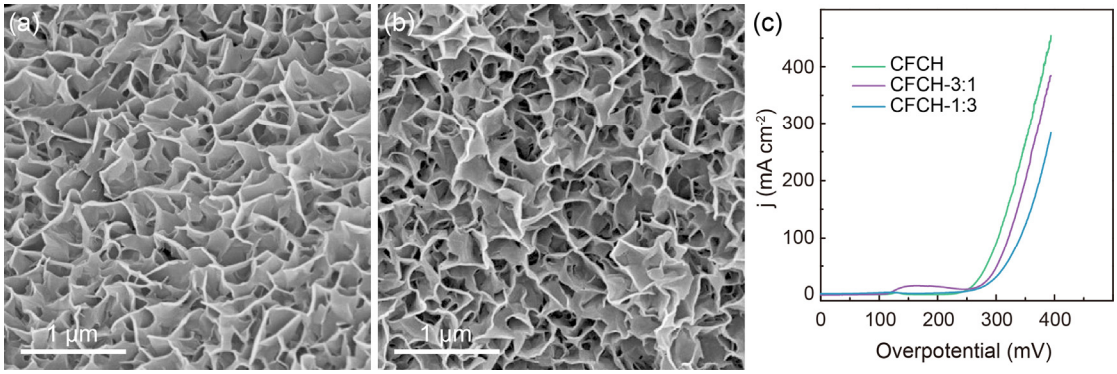

Fig. S3 SEM images of (a) CFCH-3:1 and (b) CFCH-1:3. (c) OER LSV curves of the CFCH materials with different Co/Fe ratio.

The influence of metal ratio in CFCH on OER activity is further investigated. Co/Fe ratio of 1:1 shows the best performance compared with the ratios of 3:1 (Fig. S3a) and 1:3 (Fig. S3b).

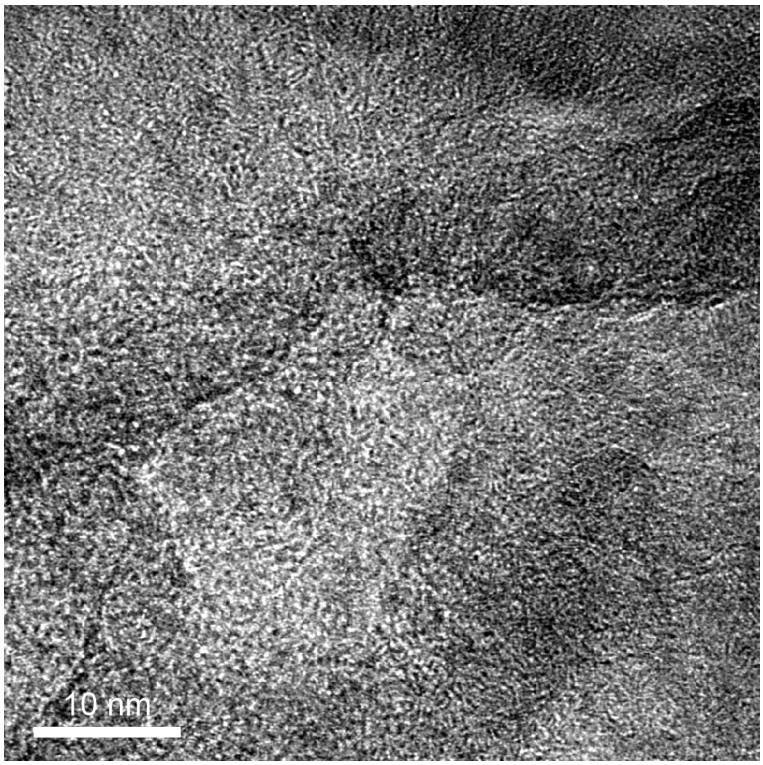

Fig. S4 HRTEM image of pristine CFCH.

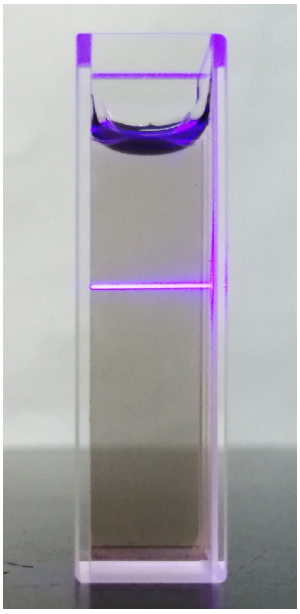

Fig. S5 Tyndall light scattering under laser irradiation for psCFCH.

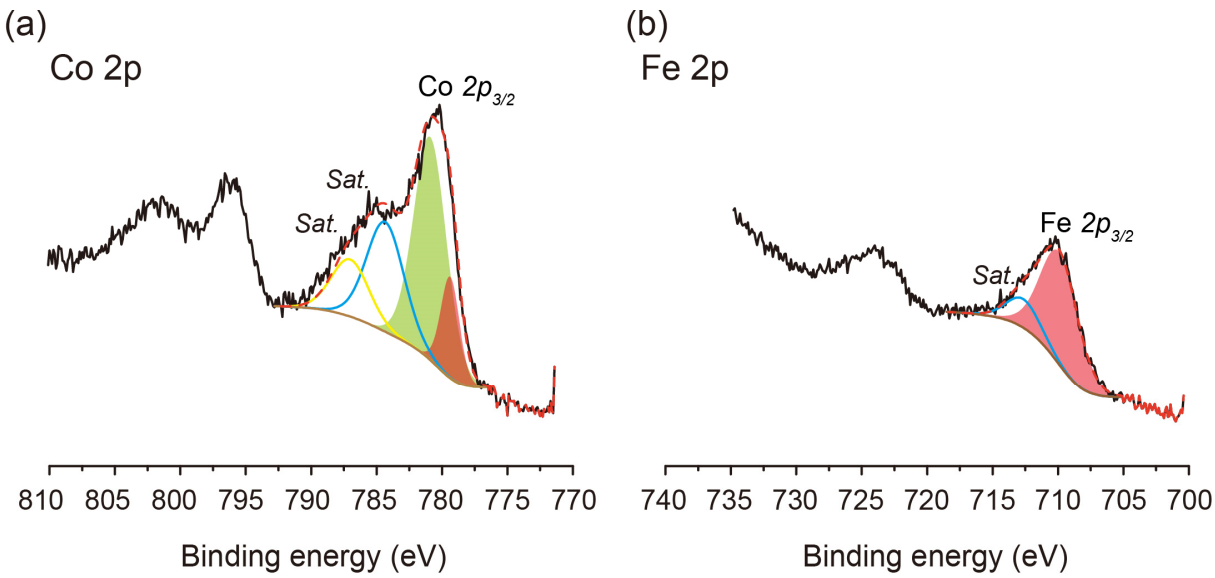

Fig. S6 XPS spectra of (a) Co *2p* and (b) Fe *2p* for CFCH.

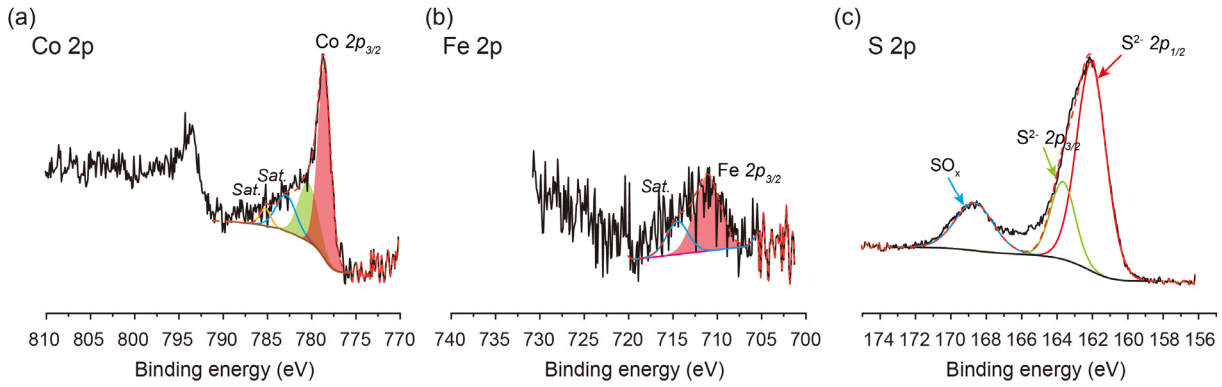

Fig. S7 XPS spectra of (a) Co *2p*, (b) Fe *2p*, and (c) S *2p* for osCFCH.

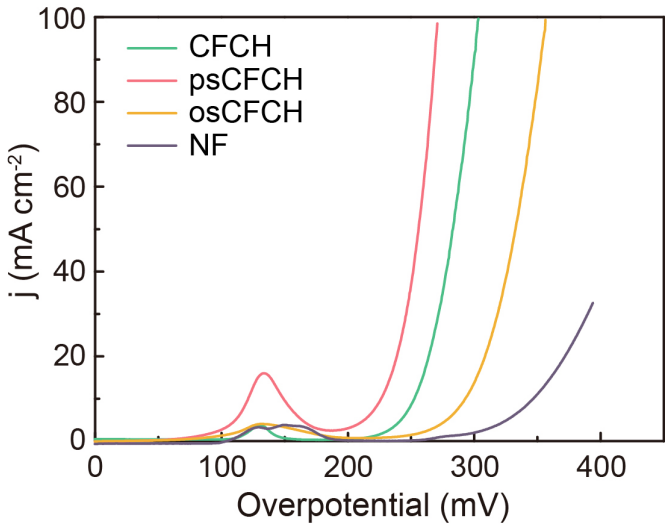

Fig. S8 Zoom-in OER LSV curves of CFCH, psCFCH, osCFCH, and NF substrate.

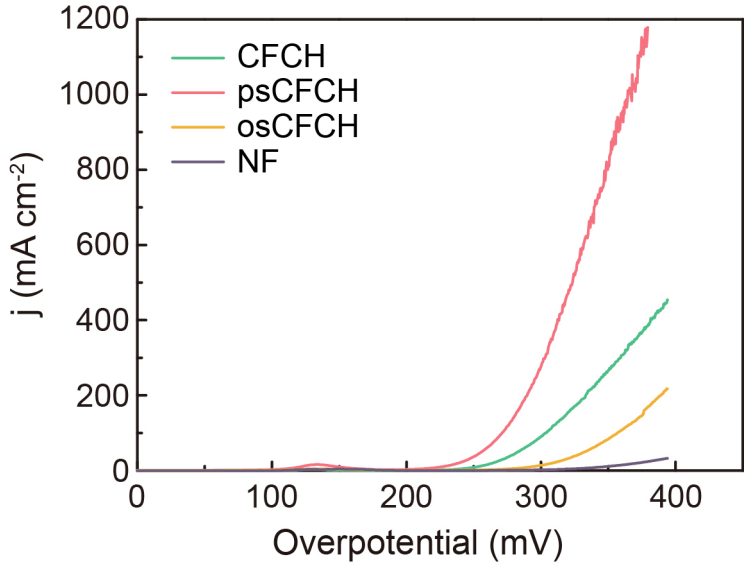

Fig. S9 Zoom-out OER LSV curves of CFCH, psCFCH, osCFCH, and NF substrate.

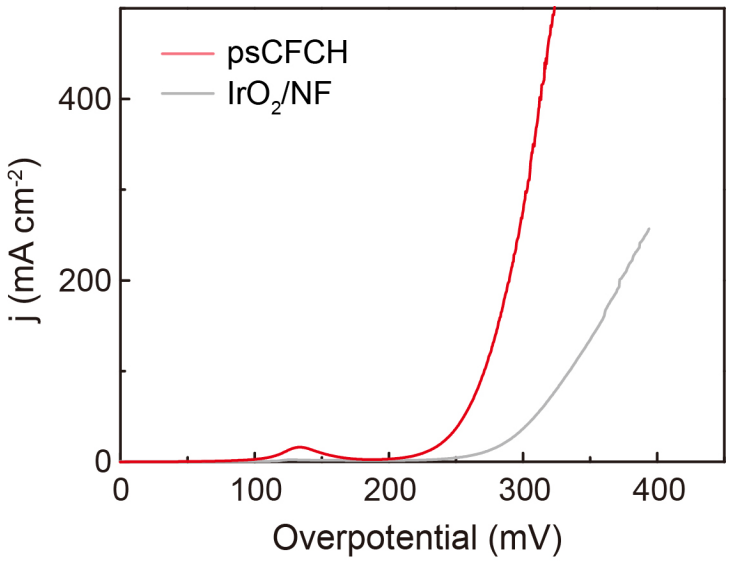

Fig. S10 OER LSV curves of psCFCH and IrO_2/NF.

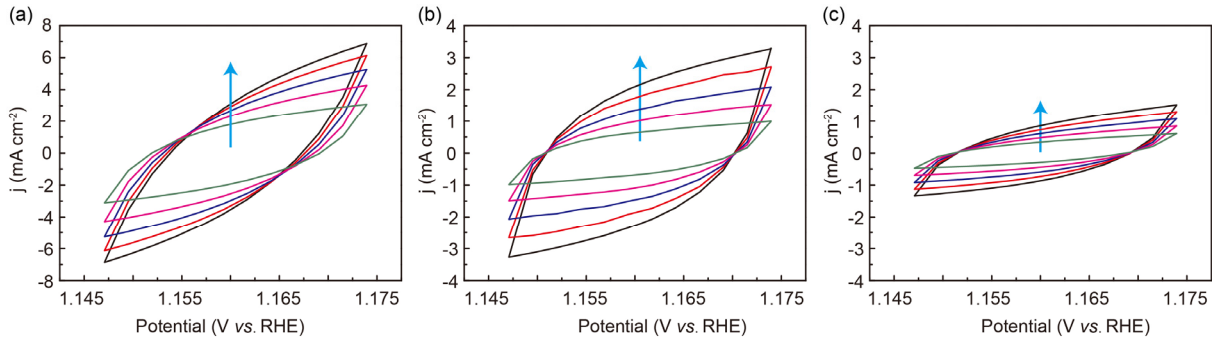

Fig. S11 Cyclic voltammograms at various scan rates of 40, 60, 80, 100, and 120 mV s^{-1} for (a) CFCH, (b) psCFCH, and (c) osCFCH.

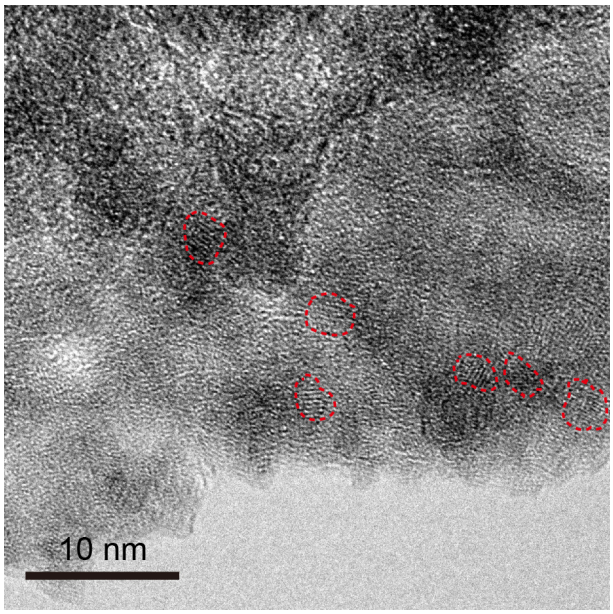

Fig. S12 TEM image of psCFCH after durability test.

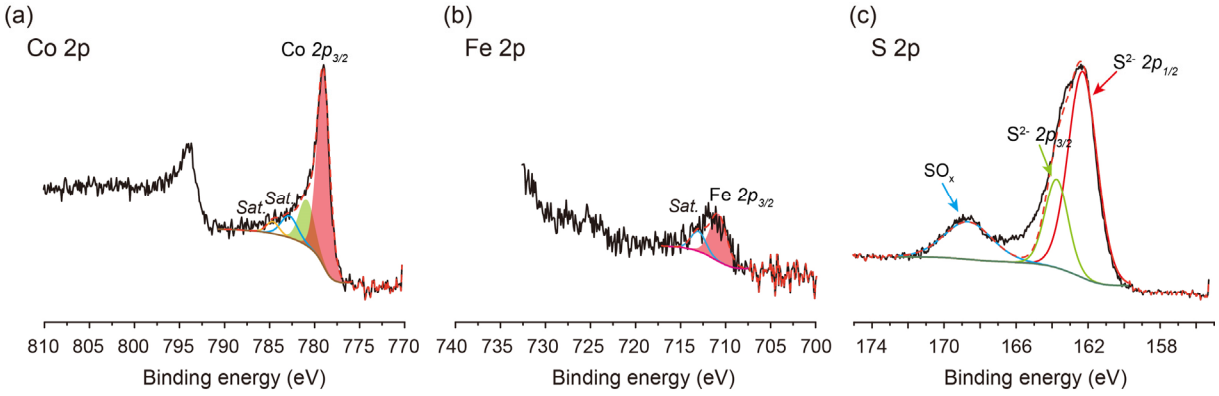

Fig. S13 XPS spectra of (a) Co *2p*, (b) Fe *2p*, and (c) S *2p* for psCFCH after durability test.

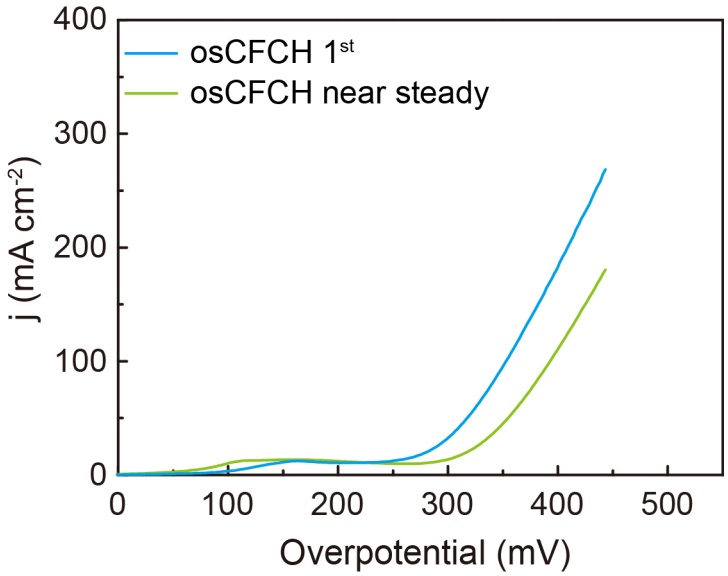

Fig. S14 OER LSV curves of osCFCH at 1st scan and near steady state. The curves are recorded without iR-compensation at a fast scan rate of 5 mV s^{-1}.

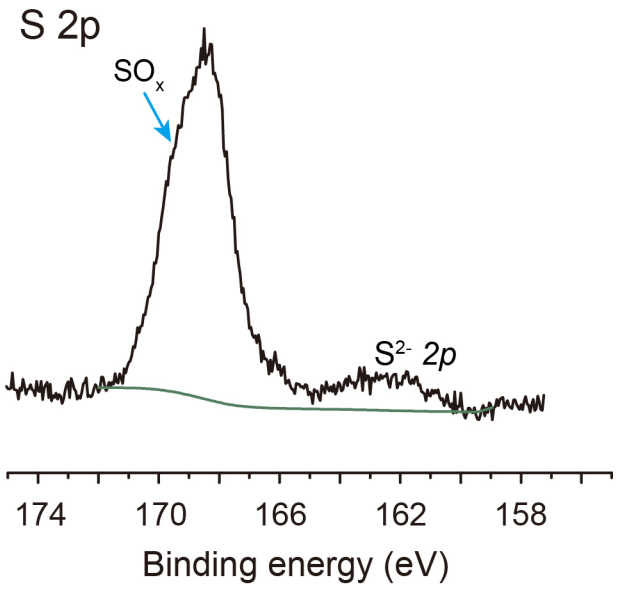

Fig. S15 XPS spectrum of S *2p* for osCFCH after durability test.

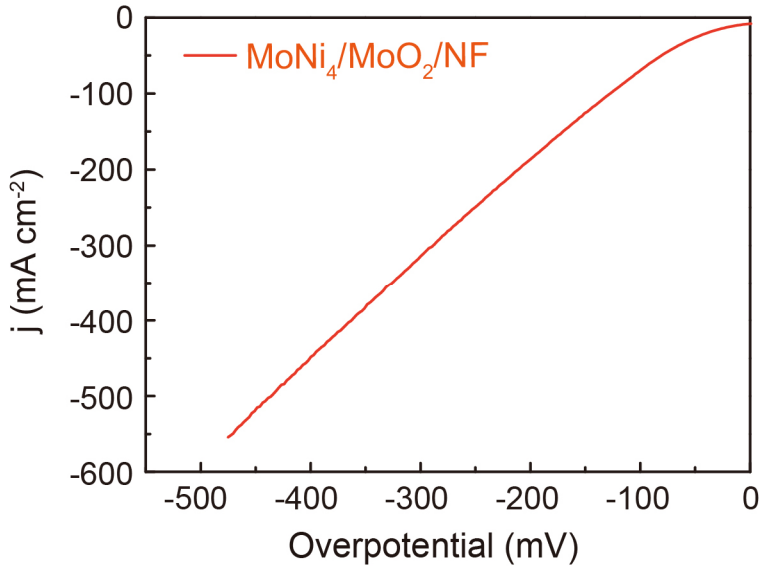

Fig. S16 HER curve of $MoNi_4/MoO_2$/NF without iR-compensation.

Table S1 Comparison of OER catalytic performance of various state-of-the-art electrocatalysts in 1 M KOH.

Catalysts	Overpotentials (mV) at various current densities			Tafel slops (mV dec^{-1})	References
	10 mA cm^{-2}	100 mA cm^{-2}	1000 mA cm^{-2}		
CFCH	**252**	**304**	**-**	**45.1**	**This work**
psCFCH	**226**	**271**	**367**	**41.3**	
osCFCH	**293**	**357**	**-**	**49.4**	
CuNiN/FeNiCu	300	400	-	45	Nat. Commun., 2018, 9, 2326.
CoO/CoFeO	297	370	-	61	Adv. Mater., 2018, 30, 1801211.
NiFe LDH-NS@DG10	210	-	-	52	Adv. Mater., 2017, 29, 1700017.
NiCo/NiCoO	332	430	-	84	Adv. Mater., 2018, 30, 1705442.
γ-CoOOH NS	300	-	-	52	Angew. Chem. Int. Ed., 2015, 54, 8722.
CoO/MnO	378	-	-	61	Angew. Chem. Int. Ed., 2017, 56, 8539.
CoFeSOH	358	-	-	74	Adv. Mater., 2017, 29, 1702327.
NiSe	320	~420	-	80	Adv. Mater., 2017, 29, 1701687.
FCCH/NF	228	252	308	42	Adv. Energy Mater., 2018, 8, 1800175.
FeCo-CoN	280	-	-	40	Adv. Mater., 2017, 29, 1704091.
pc-Ni-B_i@NB	302	-	-	52	Angew. Chem. Int. Ed., 2017, 56, 6572.
NiFeC	210	-	-	35	Adv. Mater., 2018, 30, 1705106.
NiCo-HS@G	259	318	-	49.6	Adv. Funct. Mater., 2018, 28, 1704594.
NF@NC–$CoFe_2O_4$/C NRAs	240	300	-	45	Adv. Mater., 2017, 29, 1604437.
NiFe LDH/GO	210	-	-	39	Angew. Chem. Int. Ed., 2014, 53, 7584.

NiCo-MOF/Cu foam	189	-	-	42	Nat. Energy, 2016, 1, 16184.
Co_1Mn_1CH/NF	294@30	349	~410	-	J. Am. Chem. Soc., 2017, 139, 8320.
$NiCo_2S_4$/NF	-	470	-	40.1	Adv. Funct. Mater., 2016, 26, 4661.
FeNiOOH(Se)/IF	222	279	348	-	J. Am. Chem. Soc., 2019, 141, 7005
NiFeRu-LDH	225	260	-	-	Adv. Mater., 2018, 30, 1706279.
NiCo@$NiCoO_2$/C PMRAs	366@20	~420	-	83.97	Adv. Mater., 2018, 30, 1705442.
Ir/C 20 wt%	270	-	-	40	J. Am. Chem. Soc., 2013, 135, 8452.
Ni–Fe disulfide@oxyhydroxide	230	-	-	42.6	J. Mater. Chem. A, 2017, 5, 4335.
$Co_2NiS_{2.4}(OH)_{1.2}$	279	-	-	52	J. Energy Chem., 2019, 38, 8.

Table S2 Comparison of overall water splitting performance of various state-of-the-art electrocatalysts in 1 M KOH.

Catalysts	Potentials (V) at various current densities		References
	10 mA cm^{-2}	100 mA cm^{-2}	
psCFCH // $MoNi_4/MoO_2$/NF	**1.51**	**1.62**	**This Work**
Se-(NiCo)S/OH	1.60	~2.08	Adv. Mater., 2018, 30, 1705538.
FeNiOOH(Se)/IF // $MoNi_4/MoO_2$/NF	1.55@20	~1.71	J. Am. Chem. Soc., 2019, 141, 7005
$FeSe_2$	1.72	-	Angew. Chem. Int. Ed., 2017 56, 10506.
MoS_2/Ni_3S_2 heterostructures	1.56		Angew. Chem. Int. Ed., 2016 55, 6702.
Ni-Co-P hollow nan bricks	1.62	~1.98	Energy Environ. Sci., 2018, 11, 872.
$Co_{1-x}Fe_xP$/CNT	1.5		Adv. Funct. Mater., 2017, 27, 1606635.
$NiCo_2O_4$/NF	1.84	>2.0	Adv. Funct. Mater., 2016, 26, 4661.
CoP/NCNHP	1.64	~1.95	J. Am. Chem. Soc., 2018, 140, 2610.
$NiCo_2O_4$	1.65	-	Angew. Chem. Int. Ed., 2016, 55, 6290.
NiFe/$Ni(OH)_2$/NiAl // NiMo/$Ni(OH)_2$/NiAl	1.59	-	Adv. Sci., 2017, 4, 1700084.
NiFeV-LDHs	1.591	~1.82	Small, 2018, 14, 1703257.
NiFe-NiMo	1.51	-	Nat. Commun., 2018, 9, 2014.
NiFe LDH/NF	1.7	-	Science, 2014, 345, 1593.
Co-CoO_x/CN	1.6	>2.0	J. Am. Chem. Soc., 2015, 137, 2688.
Fe–CoP	1.60	-	Adv. Mater., 2017, 729, 602441.
NiFe LDH-NS@DG	1.50@20	-	Adv. Mater., 2017, 29, 1700017.
Ni_2P/NF	1.63	-	Energy Environ. Sci., 2015, 8, 2347.
Co_3O_4 microtube arrays	1.63	~1.98	Angew. Chem. Int. Ed., 2017, 56, 1324.
Co_1Mn_1CH/NF	1.68	~1.98	J. Am. Chem. Soc., 2017, 139, 8320

Table S3 Comparison of overall solar-to-hydrogen conversion efficiency in recent reports and this work.

Electrochemical cells	Solar cells	STH efficiency	Electrolytes	References
psCFCH // $MoNi_4/MoO_2$/NF	**GaAs**	**16.99%**	**1 M KOH**	**This work**
NiFe LDH // NiFe LDH	Lead halide ($CH_3NH_3PbI_3$) perovskite 2p	12.3%	1 M NaOH	Science, 2014, 345, 1593.
CoMnO@CN	Silicon	8%	1 M KOH	J. Am. Chem. Soc., 2015, 137, 14305.
FeNiOOH(Se)/IF // $MoNi_4/MoO_2$/NF	GaAs	18.55%	1 M KOH	J. Am. Chem. Soc., 2019, 141, 7005.
Ni // Pt	PBDTTPD:PCBM/PEDOT:PSS 3jn	6.1%	1 M NaOH	Adv. Mater., 2016, 28, 3366.
MHCM // NiMoS	GaInP/GaAs/Ge 3jn	17.9%	Sea water	Adv. Mater., 2018, 30, 1707261.
NiFe LDH // CrNN	GaAs	15.1%	1 M KOH	Angew. Chem. Int. Ed., 2015, 54, 11989.
Na:$NiFeO_x$ // NiP	Lead halide ($CH_3NH_3PbI_3$) perovskite 2p	11.22%	1 M KOH	Energy Environ. Sci., 2017, 10, 121.
NiFe LDH // NiP	Lead halide ($CH_3NH_3PbI_3$) perovskite 2p	12.7%	pH 13.6/BPM/pH 0.9	Adv. Energy. Mater., 2016, 6, 1600100.
CuCoO-NW	Silicon	4.5%	1 M KOH	Adv. Funct. Mater., 2016, 26, 8555.
$NiCo_2S_4$	GaAs	18.01%	1 M KOH	Adv. Funct. Mater., 2019, 29, 1807031